

Pump-intensity-scaling of Two-Photon-Absorption and Photon Statistics of Entangled-Photon Fields

Deependra Jadoun,^{1,2} Upendra Harbola,³ Vladimir Y. Chernyak,^{4,5} and Shaul Mukamel^{1,2}

¹*Department of Chemistry, University of California, Irvine, CA 92614, USA*

²*Department of Physics and Astronomy,
University of California, Irvine, CA 92614, USA*

³*Department of Inorganic and Physical Chemistry,
Indian Institute of Science, Bangalore 560012, India*

⁴*Department of Chemistry, Wayne State University,
5101 Cass Ave, Detroit, Michigan 48202, USA*

⁵*Department of Mathematics, Wayne State University,
656 W. Kirby, Detroit, Michigan 48202, USA*

(Dated: February 17, 2025)

We use a non-perturbative theoretical approach to the parametric down-conversion (PDC) process, which generates entangled-photon field for an arbitrarily strong pump-pulse. This approach can be used to evaluate multi-point field correlation functions to compute nonlinear spectroscopic signals induced by a strong pump. The entangled-photon statistics is studied using Glauber's $g^{(2)}$ function, which helps understand the significance of the photon entanglement-time and the pump-pulse intensity on spectroscopic signals. Under the non-perturbative treatment of the entangled field, the two-photon absorption (TPA) signal shows linear to strongly non-linear growth with the pump intensity, rather than linear to quadratic scaling reported previously. An increase in the range of pump intensity for the linear scaling is observed as the pump band-width is increased. We propose an experimental scheme that can select contributions to the TPA signal that arise solely from interactions with the entangled photons, and filter out unentangled photon contributions, which are dominant at higher pump intensities, paving a way to explore the entanglement effects at higher intensities.

I. INTRODUCTION

Entanglement is a quantum mechanical effect that correlates two or more particles in a non-classical way. An entangled pair of photons, also known as quantum light, is one such example where the time-energy entanglement between the two entangled photons can be utilized in spectroscopy to gain insights into the chemical dynamics of molecules at an unprecedented resolution that is not possible with classical light [1]. Two-photon absorption (TPA) is the simplest spectroscopic technique that can demonstrate the merits of quantum light [2–4]. The entangled-photon pairs obtained by parametric-down conversion (PDC) have been employed in numerous TPA experiments [5–12]. The signal is commonly detected by the fluorescence from doubly excited molecular states [9, 13–15].

Most theoretical studies involving entangled-photons are limited to the weak pump field regime, which involves a single pair of entangled-photons interacting with the molecule [16–18]. It is experimentally challenging to observe the weak spectroscopic signal generated by isolated entangled-photon pairs [19–21]. This difficulty may be overcome by increasing the pump intensity, whereby several entangled-photon pairs can interact with the molecule. One such example of the entangled-field is the bright-squeezed vacuum [23]. However, a strong pump increases unwanted contributions that arise from molecular interactions with photons belonging to different entangled pairs that lack the quantum information of the entangled field.

A spectroscopic signal generated by the bright squeezed vacuum can be divided into two parts, denoted as inter-mode and intra-mode contributions, where the former involves both the “signal” and the “idler” modes [24], while the latter has only the “signal” or the “idler” mode contribution. Only the inter-mode part is sensitive to the photon entanglement. We have recently shown that at low pump intensities (but beyond single entangled-pair limit), the light-to-matter entanglement transfer is reduced by the presence of intra-mode contributions [25]. Recently, intense entangled beams have been employed in TPA [24] and virtual-state spectroscopy [26] to study the impact of the time-entanglement between the two modes. The intra-mode contributions dominate at large pump intensities, which can obscure the quantum effects arising from the entangled nature of the field. This causes difficulties in observing the theoretically predicted effects of photon-entanglement in experiments. An accurate description of the entangled field effects, therefore, requires using arbitrary pump-

pulse intensity (to enhance the signal) together with a spectroscopic scheme that can remove the unwanted background intra-mode contributions. This is the aim of the present work.

We use a non-perturbative approach to describe the pump field with arbitrary spectral width and intensity, which interacts with the PDC crystal to generate entangled-photon field. Starting with the effective Hamiltonian previously used by Dayan and Raymer [22, 23] to study high pump-intensity effects, we derive a system of linear integro-differential equations whose solutions with appropriate boundary conditions provide the exact correlation functions of the entangled field. Our system of equations is equivalent to the one presented in Ref. [27]. Switching to the Wigner representation of the field correlation functions allows us to extend the exact analytical solutions for infinitely narrow spectral width pump (presented, e.g., in Ref. [23]) to obtain an asymptotically exact expression for the case of a narrow, rather than an infinitely narrow, pump. We compare the “almost analytical” Wigner approach with the results obtained from a completely numerical solution and (i) show that for a sufficiently narrow pump, the two methods show excellent agreement, and (ii) identify the range of the pump spectral width, where the narrow pump solution can be safely implemented.

We use this approach to evaluate the Glauber’s $g^{(2)}$ function of entangled photons, and study the role of entanglement-time and pump spectral width on the photon-statistics of the entangled field. We further investigate the TPA signal and its scaling with the pump intensity and spectral width. We finally propose an experimental protocol that can remove the unwanted intra-mode contributions from the TPA signal.

II. THEORY

The TPA signal is given by the photon creation rate in the output (fluorescence) mode with frequency ω_f , (see Sec. I in the SI),

$$\begin{aligned}
 R(\omega_f, t) &\equiv \sum_{\lambda} \frac{d}{dt} \langle E_f^{\lambda\dagger}(t) E_f^{\lambda}(t) \rangle \\
 &= \frac{2}{\hbar^2} \text{Re} \sum_{\lambda} \sum_{i>j} \sum_{i'>j'} (\mu_{ij} \cdot \epsilon_{\lambda}) (\mu_{i'j'}^* \cdot \epsilon_{\lambda}) \int_{-\infty}^t d\tau \langle B_{ijR}^{\dagger}(t) B_{i'j'L}(\tau) \rangle e^{-i\omega_f(t-\tau)}
 \end{aligned} \tag{1}$$

Here μ_{ij} is the transition dipole moment between molecular states i and j , and ϵ_{λ} is the output mode polarization. $B_{ij} = |j\rangle\langle i|$ is the excitation operator from the i th to j th elec-

tronic molecular state, and the subscripts R and L denote “right” and “left” superoperators, respectively, defined in Liouville space through their actions on the density-matrix, [e.g, $A_L\rho = A\rho$, $A_R\rho = \rho A$ such that $A_-\rho = (A_L - A_R)\rho$][28]. The angular bracket $\langle \cdot \rangle$ denotes the trace over the combined molecule and the incoming entangled field degrees-of-freedom.

Computing $R(\omega_f, t)$ requires calculating the exciton correlation function $\langle B_{ijR}^\dagger(t)B_{i'j'L}(\tau) \rangle$. This can be done by using a modified correlation $\mathcal{G}_{ij'j'}^{RL}(t, \tau) = \langle TB_{ijR}^\dagger(t)B_{i'j'L}(\tau) \rangle$, where T is the time-ordering operator. $R(\omega_f)$ depends on the retarded ($t > \tau$) correlation function. Calculating $\mathcal{G}_{ij'j'}^{RL}(t, \tau)$ requires computationally expensive solution of several self-consistent equations in terms of single-particle (Green’s functions) propagators[28–30] for the molecule. In the following, we compute the exciton correlation function perturbatively in the (incoming) entangled field-molecule coupling by expressing the correlation function in the interaction picture.

$$\mathcal{G}_{ij'j'}^{RL}(t, \tau) = \langle TB_{ijR}^\dagger(t)B_{i'j'L}(\tau)e^{-\frac{i}{\hbar} \int d\tau_1 H_{int}-(\tau_1)} \rangle \quad (2)$$

with $H_{int}(t) = \sum_{ijq\lambda} \mu_{ij} B_{ij}^\dagger(t) E_q^\lambda(t) + h.c.$, where E_q^λ is the annihilation operator for the the incoming field with frequency ω_q and polarization ϵ_λ . All time-dependences are in the interaction picture.

The zeroth-order contribution in the perturbative expansion of Eq. (2) in H_{int} vanishes for a molecule initially in the ground state. The two leading (second and fourth) -order contributions are,

$$\begin{aligned} \overline{\mathcal{G}}_{ij'j'}^{RL}(t, \tau) \approx & \frac{2}{\hbar^2} (\mu_{i_1 j_1} \cdot \epsilon_{\lambda_1}) (\mu_{i_2 j_2}^* \cdot \epsilon_{\lambda_2}) \int d\tau_1 d\tau_2 \left[\right. \\ & \langle TE_{q_1 L}^{\lambda_1}(\tau_1) E_{q_2 R}^{\lambda_2 \dagger}(\tau_2) \rangle \langle TB_{ijR}^\dagger(t) B_{i'j'L}(\tau) B_{i_1 j_1 L}^\dagger(\tau_1) B_{i_2 j_2 R}(\tau_2) \rangle \\ + & \frac{3}{\hbar^2} (\mu_{i_3 j_3}^* \cdot \epsilon_{\lambda_3}) (\mu_{i_4 j_4}^* \cdot \epsilon_{\lambda_4}) \int d\tau_3 d\tau_4 \langle TE_{q_1 L}^{\lambda_1}(\tau_1) E_{q_2 L}^{\lambda_2}(\tau_2) E_{q_3 R}^{\lambda_3 \dagger}(\tau_3) E_{q_4 R}^{\lambda_4 \dagger}(\tau_4) \rangle \\ \times & \langle TB_{ijR}^\dagger(t) B_{i'j'L}(\tau) B_{i_1 j_1 L}^\dagger(\tau_1) B_{i_2 j_2 L}^\dagger(\tau_2) B_{i_3 j_3 R}(\tau_3) B_{i_4 j_4 R}(\tau_4) \rangle \\ - & \frac{6}{\hbar^2} (\mu_{i_3 j_3} \cdot \epsilon_{\lambda_3}) (\mu_{i_4 j_4}^* \cdot \epsilon_{\lambda_4}) \int d\tau_3 d\tau_4 \\ \times & \left(\langle TE_{q_1 L}^{\lambda_1}(\tau_1) E_{q_2 L}^{\lambda_2}(\tau_2) E_{q_3 L}^{\lambda_3 \dagger}(\tau_3) E_{q_4 R}^{\lambda_4 \dagger}(\tau_4) \rangle \langle TB_{ijR}^\dagger(t) B_{i'j'L}(\tau) B_{i_1 j_1 L}^\dagger(\tau_1) B_{i_2 j_2 L}(\tau_2) B_{i_3 j_3 L}^\dagger(\tau_3) B_{i_4 j_4 R}(\tau_4) \rangle \right) \\ + & \left. \langle TE_{q_1 L}^{\lambda_1}(\tau_1) E_{q_2 R}^{\lambda_2}(\tau_2) E_{q_3 R}^{\lambda_3 \dagger}(\tau_3) E_{q_4 R}^{\lambda_4 \dagger}(\tau_4) \rangle \langle TB_{ijR}^\dagger(t) B_{i'j'L}(\tau) B_{i_1 j_1 L}^\dagger(\tau_1) B_{i_2 j_2 R}(\tau_2) B_{i_3 j_3 R}^\dagger(\tau_3) B_{i_4 j_4 R}(\tau_4) \rangle \right] \end{aligned} \quad (3)$$

where summation over repeated indices is implied. The physical processes which give rise

to the various contributions in Eq. (3) are depicted in Fig. (1).

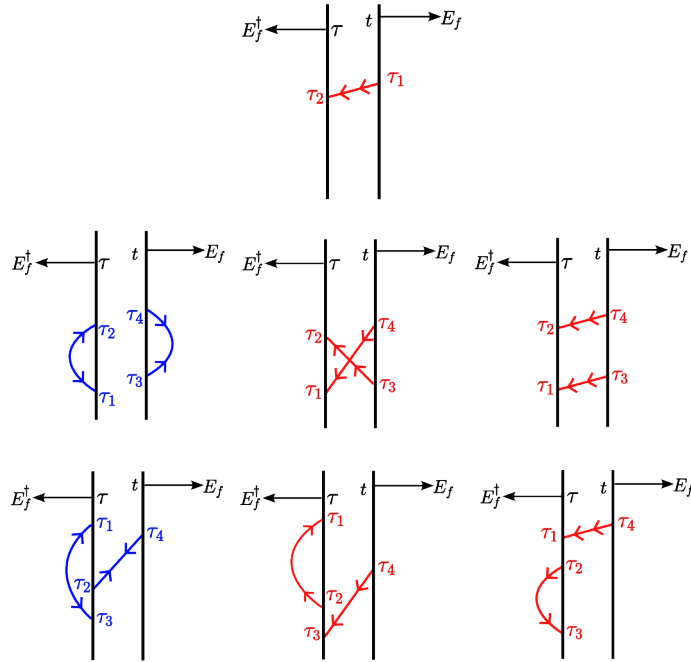


FIG. 1. Diagrams contributing to the first term (top panel), the second term (middle panel), and the third term (bottom panel) in Eq. (3). Diagrams for the last term in Eq. (3) are obtained by interchanging the left and right interactions at $\tau_i, i = 1, 2, 3, 4$, in the bottom diagram. Interactions at times t and τ represented by the horizontal arrows correspond to the observed fluorescent mode. Red (blue) curves with two arrowheads denote ordinary (anomalous), $D^{-+}(D^{--}, D^{++})$ entangled-field propagators (see discussion below Eq. (4)). Arrowheads pointing (out) into the vertical black lines represent field $(E^\dagger)E$.

The first term represents an excitation from the ground state $|g\rangle$ to the doubly excited state $|f\rangle$ by the absorption of a resonant pump photon. It could also represent the absorption of a single “idler” or “signal” photon, which has the proper energy due to the finite pump-pulse bandwidth. Hereafter, we assume that the pump-photons in the crystal output are filtered out using phase-matching and do not contribute to the first term. Note that each field operator includes both the “signal” and “idler” modes, $E_q^\lambda = E_s^\lambda(\omega_q) + E_i^\lambda(\omega_q)$. The field correlation function $\langle TE_{q_1L}^{\lambda_1}(\tau_1)E_{q_2R}^{\lambda_2\dagger}(\tau_2)\rangle$ (Section III in the SI) has four terms, where two cross terms that contain inter-mode correlations vanish. Thus, the first term in Eq. (3) only includes intra-mode photon correlations which is non-zero if the polarizations (ϵ_{λ_1} and ϵ_{λ_2}) are parallel.

The second and the third terms in Eq. (3) contain four-time field correlation functions that, by use of Wick's theorem for Boson fields, may be factorized into products of two-time field correlation functions.

$$\begin{aligned}
D_{\lambda_1\lambda_2\lambda_3\lambda_4}^{- - + + LLLR}(\tau_1, \tau_2, \tau_3, \tau_4) &= \langle TE_{q_1L}^{\lambda_1}(\tau_1)E_{q_2L}^{\lambda_2}(\tau_2)E_{q_3L}^{\lambda_3\dagger}(\tau_3)E_{q_4R}^{\lambda_4\dagger}(\tau_4) \rangle \\
&= \langle TE_{q_1L}^{\lambda_1}(\tau_1)E_{q_2L}^{\lambda_2}(\tau_2) \rangle \langle TE_{q_3L}^{\lambda_3\dagger}(\tau_3)E_{q_4R}^{\lambda_4\dagger}(\tau_4) \rangle \\
&+ \langle TE_{q_1L}^{\lambda_1}(\tau_1)E_{q_3L}^{\lambda_3\dagger}(\tau_3) \rangle \langle TE_{q_2L}^{\lambda_2}(\tau_2)E_{q_4R}^{\lambda_4\dagger}(\tau_4) \rangle \\
&+ \langle TE_{q_1L}^{\lambda_1}(\tau_1)E_{q_4R}^{\lambda_4\dagger}(\tau_4) \rangle \langle TE_{q_2L}^{\lambda_2}(\tau_2)E_{q_3L}^{\lambda_3\dagger}(\tau_3) \rangle
\end{aligned} \tag{4}$$

where a “- (+)” sign on the propagator D denotes that the corresponding field operator is $E(E^\dagger)$, for example, $D^{-+}(t, t') = \langle TE(t)E^\dagger(t') \rangle$. The first term in Eq. (4) is non-zero only when the paired modes, (q_1, q_2) and (q_3, q_4) , are different “signal” and “idler” modes. This contribution, therefore, depends on inter-mode correlations and carries information on the quantum state of both modes. The other two terms survive only when both paired modes belong to the same mode and represent intra-mode field correlations.

III. MODEL SIMULATIONS

We consider the molecular level-scheme depicted in Fig. (2), which consists of a ground state $|g\rangle$, one doubly excited state $|f\rangle$, and three intermediate singly excited states $|e_i\rangle, i = 1, 2, 3$. The signals arising from the various processes depicted in Fig. (1) are computed

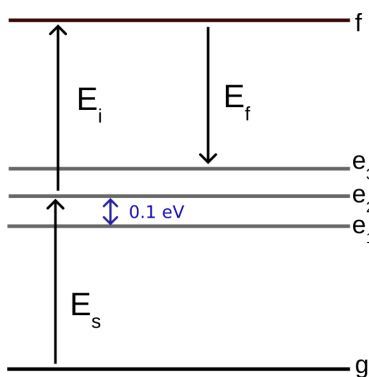


FIG. 2. Energy level scheme used in our simulations with energies $e_1=1.9 \text{ fs}^{-1}$, $e_2=2 \text{ fs}^{-1}$, $e_3=2.1 \text{ fs}^{-1}$, and $e_4=4 \text{ fs}^{-1}$.

by expanding the molecular correlation functions in Eq. (3) in molecular eigenstates, as discussed in Sec. II in the SI. The leading-order term, given by the first diagram in Fig.

(1), originates from intra-mode interactions. The other terms contain both the inter- and the intra-mode contributions, represented by the blue and the red colored field propagators, respectively. These field propagators are computed using the effective Hamiltonian approach given in Sec. III in the SI. The different contributions, $R^{(n)}$, given in Eqs. (5-10) in SI, therefore, carry quantum information regarding the entangled light field and are related to Glauber's $g^{(2)}$ function which is commonly used to describe the non-classical behavior of light[31]. $g^{(2)}(t, \tau)$ can be measured by the coincidence-counting of photons at times $t - \tau$ and t ,

$$g^{(2)}(t, \tau) = \frac{\langle E^\dagger(t - \tau)E^\dagger(t)E(t)E(t - \tau) \rangle}{\langle E^\dagger(t - \tau)E(t - \tau) \rangle \langle E^\dagger(t)E(t) \rangle}. \quad (5)$$

Integrating over t gives,

$$g^{(2)}(\tau) = \frac{1}{S(\tau)} \int \int \int \frac{d\omega_1 d\omega_2 d\omega_3}{(2\pi)^3} e^{-i(\omega_2 - \omega_3)\tau} \langle E^\dagger(\omega_1)E^\dagger(\omega_2)E(\omega_3)E(\omega_1 + \omega_2 - \omega_3) \rangle \quad (6)$$

where $\omega_4 = \omega_1 + \omega_2 - \omega_3$ and $S(\tau) = \int \frac{d\omega_1 d\omega_2 d\omega_3}{(2\pi)^3} \langle E^\dagger(\omega_1)E(\omega_4) \rangle \langle E^\dagger(\omega_2)E(\omega_3) \rangle e^{-i(\omega_2 - \omega_3)\tau}$ is a normalization factor that only includes the intra-mode field correlations. $g^{(2)}$ can be decomposed into a sum of intra-mode, $g_0^{(2)}$, and inter-mode, $g_1^{(2)}$, contributions. Both contributions decay with τ . At long τ , the normalized intra-mode part saturates to unity, while the inter-mode part vanishes.

The inter- and intra-mode components of $g^{(2)}(\tau)$ for various field entanglement times are displayed in Fig. (3). Both components show strong dependence on the entanglement time and rapidly decay as the entanglement time is decreased. At high pump intensities, the two contributions are virtually identical. However, differences show up at low pump intensities where the inter-mode contribution survives for longer delays and vanishes beyond the entanglement time. For a degenerate entangled field produced by a continuous laser field, the Glauber function is computed in Sec. III-B in the SI. The temporal profile of $g_{0/1}^{(2)}(\tau)$ is Gaussian with a time-scale, which is mainly determined by the entanglement time for low-pump intensities, while, at larger intensities, it decreases with the intensity, leading to a shorter effective entanglement time. The analytic results for the continuous field can be extended for a finite (non-zero) but large time-scale (narrow band-width) pump pulse using Wigner representation as discussed in Sec. III in the SI. The inset in Fig. (3) compares the numerical results with the semi-analytic (Wigner) results for $\sigma_p = 0.3 \text{ fs}^{-1}$.

The time-dependent Glauber function is depicted for different pump bandwidths in Fig. (4). At high pump intensities, as the bandwidth is increased, the relaxation slows down,

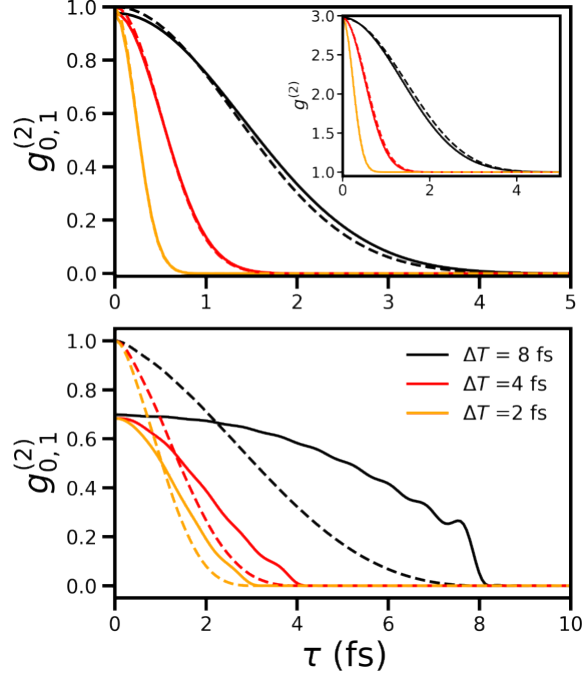


FIG. 3. Time-dependence of the inter-mode ($g_1^{(2)}$, solid) and intra-mode ($g_0^{(2)} - 1$, dashed) parts of $g^{(2)}(\tau)$ for different entanglement times, as indicated. Upper(lower) panel: for high (low) pump intensity, $I_p=3.35\times 10^{16}$ (3.35×10^{14}) W/cm². Other parameters are: $\sigma_p=0.3$ fs⁻¹, $\omega_p=4$ fs⁻¹, $\omega_s=2$ fs⁻¹, and PDC crystal length $l = 20$ μ m. The inset compares the $g^{(2)}(\tau)$ function calculated numerically (solid) with the semi-analytical (dashed) solution.

implying a longer effective entanglement time. The difference between the intra- and inter-mode components is more pronounced at low pump intensities. The relaxation of the inter-mode contribution strongly depends on the bandwidth, which is qualitatively different from the intense pump case. As the bandwidth is increased, it shows weaker dependence on τ for τ smaller than the entanglement time, and vanishes for larger τ . The relaxation in the intra-mode part also slows down with increased bandwidth but remains qualitatively the same as for the intense pump. Thus, the inter-mode part of the Glauber function directly reveals information on the field entanglement time at larger bandwidths and low pump intensities. The inset compares the numerical and the semi-analytic results for a finite band-width pump. The exact numerical method and the semi-analytic Wigner approach agree well for small $\sigma_p\Delta T < 0.2$.

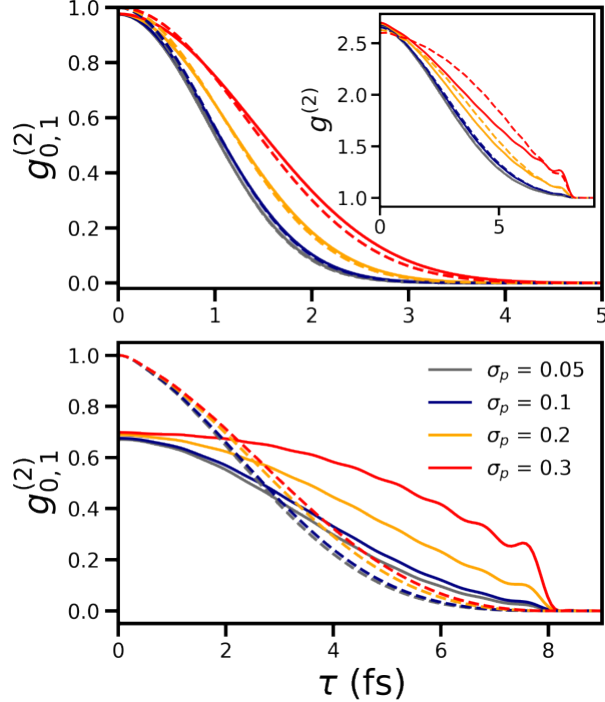


FIG. 4. The time-dependence of the inter-mode ($g_1^{(2)}$, solid) and the intra-mode ($g_0^{(2)}$, dashed) contributions for different pulse bandwidths σ_p . The upper (lower) panel shows the inter-mode and intra-mode contributions for a strong (weak) pump with the field strength of $I_p=3.35\times 10^{16}$ (3.35×10^{14}) W/cm² for the entanglement time $\Delta T = 8$ fs. The inset compares the total $g^{(2)}$ calculated numerically (solid) with semi-analytical results (dashed) for $I_p=3.35\times 10^{14}$ W/cm².

A. The TPA and its intensity scaling for a narrow-band pump

Having discussed the statistical properties of the entangled field, we now turn to the TPA process, detected by fluorescence. All processes depicted in Fig. (1) generally contribute to the signal. To simplify the analysis, we focus on a narrow-band pump resonant with the doubly excited state of the molecule. The “signal” and “idler” photon energies are bounded by the double-excitation energy. The doubly-excited state population is generated by absorbing the “signal” and “idler” photons and the fluorescence is given by the $R^{(2)}$ term in Eq. 6 of the SI, the corresponding diagrams are given in the second row in Fig. (1). The radiative transitions $|f\rangle \rightarrow |e\rangle$ and $|f\rangle \rightarrow |g\rangle$ contribute to the fluorescence from the double-excited state. Note that when the transition dipole μ_{fg} vanishes, the fluorescence solely comes from the transition $|f\rangle \rightarrow |e\rangle$ in $R^{(2)}$.

To study the scaling with the pump intensity, we consider a case where both “signal” and “idler” modes have both vertical and horizontal polarizations with equal magnitudes and all molecular transition dipoles are aligned by 45° angle to both directions so that \mathcal{M} in Eq. 6 in the SI is independent of the field polarization. All terms in $R^{(2)}$ obtained after interchanging polarizations then make the same contribution as the first term in $R^{(2)}$ and we can drop the polarization subscripts. The renormalized signal $\tilde{R}(\omega_f) = \text{Re} \{R^{(2)}(\omega_f)/\mathcal{M}^{f e_1; f e_1; f e; e g; e' g; f e'}\}$ is given by,

$$\tilde{R}(\omega_f) = \text{Im} \int \frac{d\omega_1 d\omega_2 d\omega_3}{(2\pi)^3} \frac{(48/\hbar^6)D(\omega_1, \omega_2, \omega_3, \omega_1 + \omega_2 - \omega_3)}{|\omega_1 + \omega_2 - \mathcal{E}_{fg} + i\eta|^2 (\omega_2 - \mathcal{E}_{eg} + i\eta) (\omega_3 - \mathcal{E}_{e'g} - i\eta) (\omega_f - \omega_1 - \omega_2 + \mathcal{E}_{jg} - i\eta)} \quad (7a)$$

where from Eq. (4)

$$\begin{aligned} D(\omega_1, \omega_2, \omega_3, \omega_4) &= \sum_{qq'=i,s} \langle E_q^\dagger(\omega_3) E_q(\omega_1) \rangle \langle E_{q'}^\dagger(\omega_4) E_{q'}(\omega_2) \rangle + (\omega_1 \Leftrightarrow \omega_2) \\ &+ \sum_{q \neq q'=i,s} \sum_{q_1 \neq q'_1=i,s} \langle E_q(\omega_1) E_{q'}(\omega_2) \rangle \langle E_q^\dagger(\omega_3) E_{q'_1}^\dagger(\omega_4) \rangle. \end{aligned} \quad (7b)$$

For a weak pump, where only a single entangled-photon pair interacts with the molecule, only the last term in Eq. (7b) survives.

The first two terms, therefore, represent intra-mode contributions corresponding to the two rightmost diagrams in the middle panel in Fig. (1).

Figure (5) depicts $\tilde{R}(\omega_f)$ for a model molecule with one $|f\rangle$ state and three singly-excited states having energies $E_f = 4fs^{-1}$, $E_{e_1} = 1.9fs^{-1}$, $E_{e_2} = 2.0fs^{-1}$, $E_{e_3} = 2.1fs^{-1}$ above the ground state $|g\rangle$. The three peaks represent transitions from $|f\rangle$ to the three intermediate states. The inter-mode contribution is shown by the dashed curves for two different pump intensities. The relative weight of the inter-mode contribution depends on the pump amplitude and grows as the pump intensity is decreased. This is because the probability that the molecule interacts with two photons of an entangled-pair increases at lower intensities.

The variation of the TPA signal with the pump intensity $I_p = c\epsilon_0 n_p |\mathcal{E}_p|^2/2$, where \mathcal{E}_p is the pump pulse amplitude, and n_p is the refractive index of the PDC crystal for the pump-pulse, c is the speed of light, and ϵ_0 is the permittivity of free space, at the resonant frequency $\omega_s = 2.0 \text{ fs}^{-1}$ is shown in Fig. (6). The inter-mode contributions grow linearly over a wide range of pump intensity and dominates over the intra-mode contributions that grow quadratically. However, for larger intensities, both contributions grow nonlinearly,

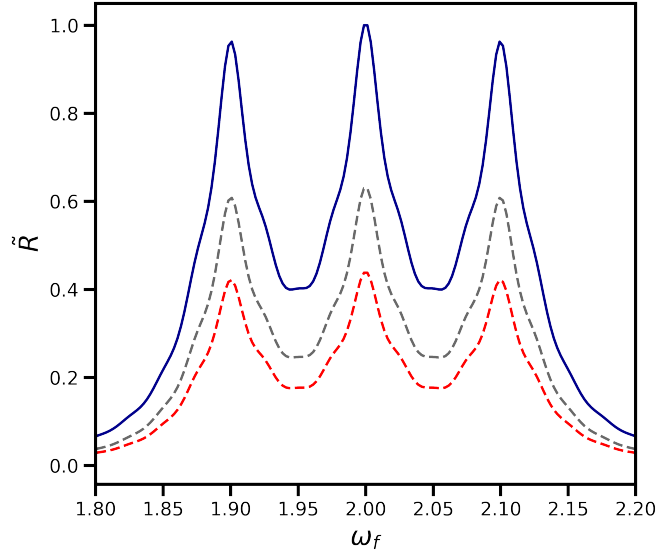


FIG. 5. Normalized TPA signal from the model molecule (Eq. 7a). The dashed-red (grey) curve is the inter-mode contribution for $I_p=3.73\times 10^{13}$ (9.33×10^{12}) W/cm^2 . Here $E_f = 4fs^{-1}$, $E_{e1} = 1.9fs^{-1}$, $E_{e2} = 2.0fs^{-1}$, $E_{e3} = 2.1fs^{-1}$, $\sigma_p = 0.1fs^{-1}$, $\eta=0.015$, $T_e=13.33$ fs.

while the inter-mode contribution remains higher. The TPA cross-section grows by orders of magnitude as the pump band-width is reduced, however the range of pump intensity over which the inter-mode contribution dominates decreases slowly with increasing band-width. PDC parameters for the LiNbO_3 are considered in calculating the TPA signal [32]. The refractive indices for the considered photon frequencies in the PDC crystal are obtained following the procedure in Ref. [33]. The value of the pump intensity beyond which nonlinear effects become significant for three commonly used PDC crystals at different pump spectral width are given in the Table.

The inter-mode contributions reveal the quantum nature of light. For example, information regarding the entanglement time and the linear variation of the signal over an order-of-magnitude larger intensity range. These contributions dominate at lower pump intensities but are masked by intra-mode processes at higher intensities, making it hard to take full advantage of the quantum light. In the next section, we propose a setup that removes the intra-mode contributions at all pump intensities.

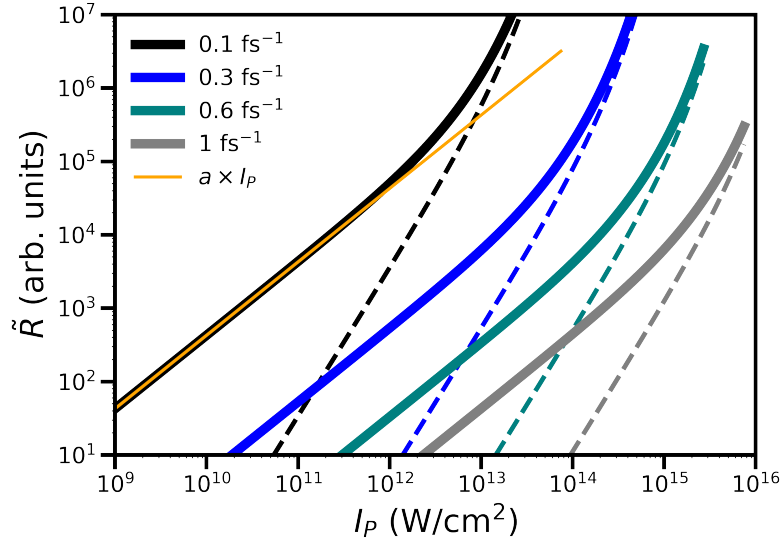


FIG. 6. Variation of the TPA signal for $\omega_f = 2 \text{ fs}^{-1}$ with pump-field intensity. The curves (top to bottom) denote the total signal calculated using Eq. (7a) for pump band-widths $\sigma_p = 0.1 \text{ fs}^{-1}$, 0.3 fs^{-1} , 0.6 fs^{-1} , and 1.0 fs^{-1} , respectively. The dashed curves show intra-mode contributions. The orange line is the fit $\tilde{R} = 2.35 \times 10^{-8} I_p$. The entanglement time is $T_e = 13.33 \text{ fs}$, $\bar{n}_s = \bar{n}_i = 2.24$, $n_p = 2.361$, and $\chi_{eff}^{(2)} = 4.6 \text{ pm/V}$.

Crystal	σ_p			
	0.1 (fs ⁻¹)	0.3 (fs ⁻¹)	0.6 (fs ⁻¹)	1 (fs ⁻¹)
LiNbO₃ ($n_i=2.24$, $n_p=2.36$, $\chi_{eff}^{(2)}=4.6 \text{ pm/V}$)	5×10^{11}	7.5×10^{12}	5×10^{13}	4×10^{14}
LiTaO₃ ($n_i=2.14$, $n_p=2.23$, $\chi_{eff}^{(2)}=0.85 \text{ pm/V}$)	1.5×10^{13}	2×10^{14}	1.5×10^{15}	8×10^{15}
KNbO₃ ($n_i=2.13$, $n_p=2.24$, $\chi_{eff}^{(2)}=10.8 \text{ pm/V}$)	1.1×10^{11}	1.2×10^{12}	8×10^{12}	1.4×10^{13}

TABLE I. Pump intensities (in W/cm^2) at which linear-to-nonlinear crossover appears for different crystals and pulse widths are depicted.

B. Filtering out the intra-mode contributions

We now present an experimental technique that filters out the unwanted (classical) intra-mode contributions from the TPA signal. The inter- and intra-mode processes have different contributions, as shown in Fig. (5) and (6), and the latter dominate at higher pump inten-

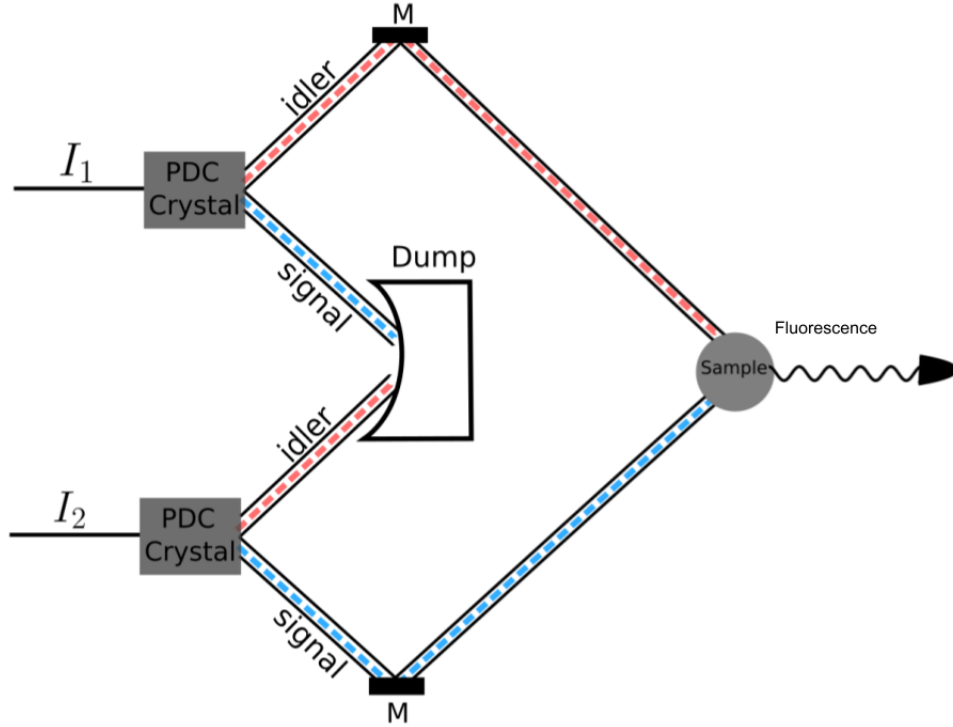


FIG. 7. Schematic setup that can be used to generate TPA signal that only includes intra-mode contributions. The s and i photons from two different entangled photon pairs are utilized. The use of identical pump and the PDC crystal ensure the generated entangled photon pairs are statistically identical to those generated by a single PDC crystal but uncorrelated.

sities. Thus, in order to take full advantage of the quantum nature of the entangled light, these contributions should be removed.

The inter-mode contributions vanish for a light field with no entangled modes. We can thus replace the “signal” and “idler” pulses with two uncorrelated pulses of the same intensity and then subtract this signal from that obtained using the entangled light. This will remove the intra-mode contributions. However, two conditions must be satisfied: bandwidths and the statistics (as determined by Glauber function) of the uncorrelated “signal” and “idler” modes must be the same as obtained from the actual PDC process. The simplest way to achieve this would be by utilizing two identical PDC crystals to generate statistically identical pairs of “signal” and “idler” pulses. We then select the “signal” pulse from one pair and the “idler” pulse from the other pair. These pulses are obviously not entangled, but are statistically identical to the entangled pulses and, upon interaction with the molecule,

generate the signal, as depicted schematically in Fig. (7). This signal will only have the intra-mode contributions since the two modes are not correlated. The signal due to inter-mode contributions is obtained by subtracting this signal from the total signal generated using entangled light, i.e., the signal measured in the presence of only one of the PDC crystals.

IV. CONCLUSION

Two-photon-absorption with an entangled photon field is a weak process. The advantage of entangled light is limited to lower pump intensities where contribution from interaction with entangled photons can outweigh contribution from non-entangled photons by orders of magnitude. This range of pump intensities can be enhanced by using a pump-pulse with a broader band-width, at the cost of signal intensity. At higher intensities, both contributions are almost equal but can be separated using the proposed experimental scheme.

Finally, we note that (i) The effective Hamiltonian used in the present study and elsewhere [22, 23], can be derived in a clean way from an effective action of the low-frequency electromagnetic (EM) field for strong pump (the weak pump perturbative expansion of the effective action has been introduced in [16]) by considering the complete perturbative expansion for the solution of the Dyson equation and neglecting the fast-oscillating (non-RWA) terms, whose contributions can be neglected, (ii) By applying the Kirchhoff-integral approach to the correlation functions of the field, together with the semiclassical (in linear optics known as eikonal) expressions for the Green functions of the Maxwell equations, one can explicitly express the entangled field correlation functions at the experimental sample in terms of their at-the-PDC-crystal counterpart, with those expressions carefully describing the optical experimental setup, *e.g.*, lenses, mirrors, delay lines, etc., thus providing the actual values (including pre-factors) of the measured signal. However, the aforementioned results go beyond the scope of this paper and will be addressed elsewhere.

ACKNOWLEDGMENTS

We thank Victor M. Freixas for the helpful discussion. U.H. acknowledges support from the Science and Engineering Board, India, under Grant No. CRG/2020/0011100 and the

Fulbright-Nehru Academic and Excellence Fellowship, 2023-24, sponsored by the U.S. Department of State and the United State-India Education Foundation. V.Y.C. and S.M. gratefully acknowledge the support of the US Department of Energy, Office of Science, Basic Energy Sciences Award DES0022134, which has primarily funded this work. S.M. gratefully acknowledges the support of the National Science Foundation through Grant No. CHE-2246379.

DISCLOSURE

The authors declare no conflicts of interest.

DATA AVAILABILITY STATEMENT

Data underlying the results presented in this paper are not publicly available at this time but may be obtained from the authors upon reasonable request.

-
- [1] Shaul Mukamel, *et al*, *J. Phys. B: At. Mol. Opt. Phys.* **53**, 072002 (2020).
 - [2] L. Gilles and P. L. Knight, *Phys. Rev. A* **48**, 1582 (1993).
 - [3] J. Gea-Banacloche, *Phys. Rev. Lett.* **62**, 1603 (1989).
 - [4] T. Landes, M. G. Raymer, M. Allgaier, S. Merkouche, B. J. Smith, and A. H. Marcus, *Opt. Express* **29**, 20022 (2021).
 - [5] K. M. Parzuchowski, A. Mikhaylov, M. D. Mazurek, R. N. Wilson, D. J. Lum, T. Gerrits, C. H. Camp, Jr., M. J. Stevens, and R. Jimenez, *Phys. Rev. Applied.* **15**, 044012 (2021).
 - [6] B. P. Hickam, M. He, N. Harper, S. Szoke, and S. K. Cushing, *J. Phys. Chem. Lett.*, vol. 13, no. 22, pp. 4934–4940, 2022.
 - [7] S. Corona-Aquino, O. Calderón-Losada, M. Y. Li-Gómez, H. Cruz-Ramirez, V. Álvarez-Venicio, M. D. P. Carreon-Castro, R. de J. León-Montiel, and A. B. U’Ren, *J. Phys. Chem. A*, vol. 126, no. 14, pp. 2185–2195, 2022.
 - [8] D. Tabakaev, M. Montagnese, G. Haack, L. Bonacina, J.-P. Wolf, H. Zbinden, and R. T. Thew, *Phys. Rev. A*, vol. 103, no. 3, p. 033701, 2021.
 - [9] D.-Ik Lee, T. Goodson III, *J. Phys. Chem. B*, **110**, 25582 (2006).

- [10] L. Upton, M. Harpham, O. Suzer, M. Richter, S. Mukamel, and T. Goodson III, *J. Phys. Chem. Lett.* **4**, 2046 (2013).
- [11] O. Varnavski, B. Pinsky, and T. Goodson III, *J. Phys. Chem. Lett.* **8**, 388 (2017).
- [12] M. R. Harpham, Ö. Süzer, C. Ma, P. Bäuerle, and T. Goodson III, *J. Am. Chem. Soc.* **131**, 973 (2009).
- [13] A. R. Guzman, M. R. Harpham, Özgün Süzer, M. M. Haley, and T. G. Goodson III, *J. Am. Chem. Soc.* **132**, 7840 (2010).
- [14] D. Tabakaev, A. Djorovic, L. La Volpe, G. Gaulier, S. Ghosh, L. Bonacina, J.-P. Wolf, H. Zbinden, and R.T. Thew, *Phys. Rev. Lett.* **129**, 183601 (2022).
- [15] T. Landes, M. Allgaier, S. Merkouche, B. J. Smith, A. H. Marcus, and M. G. Raymer, *Phys. Rev. Res.* **3**, 033154 (2021).
- [16] M. Kizmann, H. K. Yadalam, V. Chernyak, and S. Mukamel, *Proc. Natl. Acad. Sci. U.S.A.*, **120**(30), e2304737120 (2023).
- [17] J. P. V.-Monsalve, O. C.-Losada, M. N. Portela, and A. Valencia, *J. Phys. Chem. A* **121**(41), 7869 (2017).
- [18] J. Gea-Banacloche, *Phys. Rev. Lett.* **62**, 1603 (1989).
- [19] T. Landes, B. J. Smith, M. G. Raymer, arXiv:2404.16342
- [20] M. G. Raymer, T. Landes, A. H. Marcus, *J. Chem. Phys.* **155**, 081501 (2021).
- [21] A. Mikhaylov, R. N. Wilson, K. M. Parzuchowski, M. D. Mazurek, C. H. Camp Jr., M. J. Stevens, and R. Jimenez, *J. Phys. Chem. Lett.* **13**, 1489 (2022)
- [22] B. Dayan, *Phys. Rev. A* **76**, 043813 (2007).
- [23] M. G. Raymer and T. Landes, *Phys. Rev. A* **106**, 013717 (2022).
- [24] J. Svozilik, J. Peřina Jr., and R. de J. León-Montiel, *Chem. Phys.*, vol. 510, pp. 54–59, 2018.
- [25] U. Harbola, L. Candelori, J. R. Klien, V. Chernyak, and S. Mukamle, To appear in *AVS Quantum* (2023).
- [26] J. Svozilik, J. Peřina, and R. de J. León-Montiel, *JOSA B*, vol. 35, no. 2, pp. 460–467, 2018.
- [27] A. Christ, B. Brecht, W. Mauerer, and C. Silberhorn, *New Journal of Physics* **15**, 053038 (2013).
- [28] U. Harbola, S. Mukamel, *Phys. Rep.* **465** (5), 191 (2008).
- [29] U. Harbola and S. Mukamel, *J. Chem. Phys.* **124**, 044106 (2006).
- [30] G. Onida, L. Reining, and A. Rubio, *Rev. Mod. Phys.*, **74**, 601 (2002).

- [31] R. J. Glauber, *Phys. Rev.* **130**, 2529 (1963).
- [32] I. Shoji, T. Kondo, A. Kitamoto, M. Shirane, and R. Ito, *JOSA B* **14**, 2268 (1997).
- [33] G. J. Edwards and M. Lawrence, *Opt Quant Electron*, vol. 16, pp. 373–375, 1984.

Supplementary Information: Pump-intensity-scaling of Two-photon-Absorption and Photon Statistics of Entangled-Photon Fields

Deependra Jadoun,^{1,2} Upendra Harbola,³ Vladimir Y. Chernyak,^{4,5} and Shaul Mukamel^{1,2}

¹*Department of Chemistry, University of California, Irvine, CA 92614, USA*

²*Department of Physics and Astronomy, University of California, Irvine, CA 92614, USA*

³*Department of Inorganic and Physical Chemistry,
Indian Institute of Science, Bangalore 560012, India*

⁴*Department of Chemistry, Wayne State University,
5101 Cass Ave, Detroit, Michigan 48202, USA*

⁵*Department of Mathematics, Wayne State University,
656 W. Kirby, Detroit, Michigan 48202, USA*

(Dated: February 17, 2025)

I. DERIVATION OF EQ. 1 IN THE MAIN TEXT

The molecular system interacting with the radiation field is represented by the Hamiltonian,

$$H = \sum_i \mathcal{E}_i B_{ii} + \sum_s \hbar \omega_s E_s^\dagger E_s + \sum_{s,i>j} (\mu_{ij}^s B_{ij}^\dagger E_s + h.c.) + \mathcal{H} \quad (1)$$

where \mathcal{E}_i is the energy of the i th molecular state $|i\rangle$, $B_{ij} = |j\rangle\langle j|$ is the exciton operator, μ_{ij} is the transition dipole-matrix element between states $|i\rangle$ and $|j\rangle$, $E_s^\dagger(E_s)$ is the boson creation (annihilation) operator for the detected (fluorescence) field mode with frequency ω_s . The third term represents interaction of the detected mode with the molecule, and the last term is the Hamiltonian of the incoming field that prepares the electronic excitation and its interaction with the molecule. In our simulations, we assume an entangled-photon field described by Hamiltonian \mathcal{H} which needs not be specified at this point.

The signal is defined by the rate of change of intensity in the detected mode ω_s .

$$R(\omega_s, t) = \frac{d}{dt} \langle E_s^\dagger(t) E_s(t) \rangle = \frac{i}{\hbar} \langle [H, E_s^\dagger(t) E_s(t)] \rangle = -\frac{2}{\hbar} \text{Im} \sum_{i>j} \mu_{ij}^s \langle B_{ij}^\dagger(t) E_s(t) \rangle \quad (2)$$

where $\langle \cdot \rangle$ denotes average over the full Hilbert space of H . We assume weak interaction with the detected mode and compute the correlation $\langle B_{ij}^d ag(t) E_s(t) \rangle$ to leading order in the interaction. This gives,

$$\langle B_{ij}^\dagger(t) E_s(t) \rangle = \frac{-i}{\hbar} \sum_{i' < j'} \mu_{i'j'}^{s'} \int_{-\infty}^t d\tau \langle B_{ij}^\dagger(t) B_{i'j'}^\dagger(\tau) \rangle \langle E_s(t) E_{s'}^\dagger(\tau) \rangle, \quad (3)$$

where the time evolution is now in the interaction picture: molecular operators evolve with the Hamiltonian $\sum_i \mathcal{E}_i B_{ii} + \mathcal{H}$ and the field operators evolve with free-field Hamiltonian, $E_s(t) = E_s e^{-i\omega_s t}$, leading to $\langle E_s(t) E_{s'}^\dagger(\tau) \rangle = \delta_{ss'} e^{-i\omega(t-\tau)}$. Substituting this in Eq. (3), Eq. (2) finally results in Eq. 1 of the main text.

II. CONTRIBUTIONS OF THE DIAGRAMS GIVEN IN FIG. 1

For a fixed time ordering $\tau_1 > \tau_2 > \tau_3 > \tau_4$, different dipole correlations can be evaluated in terms of molecular state energies as,

$$\begin{aligned} \langle B_{ijR}^\dagger(t) B_{i'j'L}(\tau) B_{i_1j_1L}^\dagger(\tau_1) B_{i_2j_2R}(\tau_2) \rangle &= \delta_{jj'} \delta_{i_2} \delta_{i'i_1} \delta_{j_1g} \delta_{j_2g} e^{i\mathcal{E}_{ij}t} e^{-i\mathcal{E}_{i'j'}\tau} e^{-i\mathcal{E}_{i_2j_2}\tau_2} e^{i\mathcal{E}_{i_1j_1}\tau_1} \\ \langle T B_{ijR}^\dagger(t) B_{i'j'L}(\tau) B_{i_1j_1L}^\dagger(\tau_1) B_{i_2j_2L}^\dagger(\tau_2) B_{i_3j_3R}(\tau_3) B_{i_4j_4R}(\tau_4) \rangle &= \delta_{jj'} \delta_{i'i_1} \delta_{i_3} \delta_{j_3i_4} \delta_{j_4g} \delta_{i_2j_2} \delta_{j_2g} \\ &e^{-i\mathcal{E}_{i_4g}\tau_4} e^{-i\mathcal{E}_{i_3j_3}\tau_3} e^{i\mathcal{E}_{ij}t} e^{-i\mathcal{E}_{i'j'}\tau} e^{i\mathcal{E}_{i_1j_1}\tau_1} e^{i\mathcal{E}_{i_2g}\tau_2} \\ \langle B_{ijR}^\dagger(t) B_{i'j'L}(\tau) B_{i_1j_1L}^\dagger(\tau_1) B_{i_2j_2L}(\tau_2) B_{i_3j_3L}^\dagger(\tau_3) B_{i_4j_4R}(\tau_4) \rangle &= \delta_{jj'} \delta_{i'i_1} \delta_{i_4} \delta_{j_1j_2} \delta_{j_4g} \delta_{i_2i_3} \delta_{j_3g} \\ &e^{-i\mathcal{E}_{i_4g}\tau_4} e^{i\mathcal{E}_{ij}t} e^{-i\mathcal{E}_{i'j'}\tau} e^{i\mathcal{E}_{i_1j_1}\tau_1} e^{-i\mathcal{E}_{i_2j_2}\tau_2} e^{i\mathcal{E}_{i_3g}\tau_3} \\ \langle T B_{ijR}^\dagger(t) B_{i'j'L}(\tau) B_{i_1j_1L}^\dagger(\tau_1) B_{i_2j_2L}(\tau_2) B_{i_3j_3L}^\dagger(\tau_3) B_{i_4j_4R}(\tau_4) \rangle &= \delta_{jj'} \delta_{i'i_1} \delta_{i_4} \delta_{j_1j_2} \delta_{j_4g} \delta_{i_2i_3} \delta_{j_3g} \\ &e^{-i\mathcal{E}_{i_4g}\tau_4} e^{i\mathcal{E}_{ij}t} e^{-i\mathcal{E}_{i'j'}\tau} e^{i\mathcal{E}_{i_1j_1}\tau_1} e^{-i\mathcal{E}_{i_2j_2}\tau_2} e^{i\mathcal{E}_{i_3g}\tau_3} \\ \langle B_{ijR}^\dagger(t) B_{i'j'L}(\tau) B_{i_1j_1L}^\dagger(\tau_1) B_{i_2j_2R}(\tau_2) B_{i_3j_3R}^\dagger(\tau_3) B_{i_4j_4R}(\tau_4) \rangle &= \delta_{jj'} \delta_{i_2i} \delta_{i_1i'} \delta_{j_2j_3} \delta_{i_4i_3} \delta_{j_4g} \delta_{j_1g} \\ &e^{-i\mathcal{E}_{i_4g}\tau_4} e^{i\mathcal{E}_{i_3j_3}\tau_3} e^{-i\mathcal{E}_{i_2j_2}\tau_2} e^{i\mathcal{E}_{ij}t} e^{-i\mathcal{E}_{i'j'}\tau} e^{i\mathcal{E}_{i_1g}\tau_1} \end{aligned} \quad (4)$$

where the subscripts i_1, i_2 , etc., denote molecular states, $|g\rangle, |e\rangle, |e'\rangle, \dots, |f\rangle$ with energies $\mathcal{E}_g, \mathcal{E}_e, \mathcal{E}_e', \dots, \mathcal{E}_f$, respectively..

By substituting Eq. (4) in Eq. (3) in the main text and then in Eq. (1) in the main text, the

signal can be recast as, $R(\omega_s) = \sum_{n=1,6} \text{Re } R^{(n)}(\omega_s)$, with

$$R^{(1)}(\omega_s) = \frac{4}{\hbar^2} \sum_{\{\lambda\}} \mathcal{M}_{\lambda\lambda\lambda_1\lambda_2}^{ij;ij;ig;ig} \int \frac{d\omega_1}{2\pi} \frac{iD_{\lambda_1\lambda_2}^{-+LR}(\omega_1, \omega_1)}{|\omega_1 - \mathcal{E}_{ig} + i\eta|^2(\omega_s - \omega_1 + \mathcal{E}_{jg} - i\eta)} \quad (5)$$

$$R^{(2)}(\omega_s) = \frac{12}{\hbar^6} \sum_{\{\lambda\}} \int \frac{d\omega_1 d\omega_2 d\omega_3}{(2\pi)^3} \frac{(-i)\mathcal{M}_{\lambda\lambda\lambda_1\lambda_2\lambda_3\lambda_4}^{fj;fj;fe;eg;e'g;fe'} D_{\lambda_1\lambda_2\lambda_3\lambda_4}^{-++LLRR}(\omega_1, \omega_2, \omega_3, \omega_1 + \omega_2 - \omega_3)}{(\omega_2 - \mathcal{E}_{eg} + i\eta)|\omega_1 + \omega_2 - \mathcal{E}_{fg} + i\eta|^2(\omega_3 - \mathcal{E}_{e'g} - i\eta)} \quad (6)$$

$$\times \frac{1}{(\omega_s - \omega_1 - \omega_2 + \mathcal{E}_{jg} - i\eta)} + (\lambda_1 \Leftrightarrow \lambda_2) + (\lambda_3 \Leftrightarrow \lambda_4) + (\lambda_1 \Leftrightarrow \lambda_2, \lambda_3 \Leftrightarrow \lambda_4)$$

$$R^{(3)}(\omega_s) = \sum_{\{\lambda\}} \int \frac{d\omega_1 d\omega_2 d\omega_3}{(2\pi)^3} \frac{(24i/\hbar^6)\mathcal{M}_{\lambda\lambda\lambda_1\lambda_2\lambda_3\lambda_4}^{ij;ij;i'j';i'j';i'g;ig} D_{\lambda_1\lambda_2\lambda_3\lambda_4}^{-++LLLR}(\omega_1, \omega_1 - \omega_2 - \omega_3, \omega_2, \omega_3)}{(\omega_2 + \mathcal{E}_{i'g} - i\eta)(\omega_1 - \omega_3 + \mathcal{E}_{jg} - i\eta)(\omega_3 - \mathcal{E}_{i'j'} - \mathcal{E}_{ig} + i\eta)(\omega_3 - \mathcal{E}_{ig} - i\eta)} \quad (7)$$

$$\times \frac{1}{(\omega_3 - \omega_s + \mathcal{E}_{j'g} + i\eta)} + (\lambda_1 \Leftrightarrow \lambda_3)$$

$$R^{(4)}(\omega_s) = \sum_{\{\lambda\}} \int \frac{d\omega_1 d\omega_2 d\omega_3}{(2\pi)^3} \frac{(24i/\hbar^6)\mathcal{M}_{\lambda\lambda\lambda_1\lambda_2\lambda_3\lambda_4}^{e'g;e'g;fe;fe';eg} D_{\lambda_1\lambda_2\lambda_3\lambda_4}^{-++LLLR}(\omega_1, \omega_1 - \omega_2 - \omega_3, \omega_2, \omega_3)}{(\omega_2 + \mathcal{E}_{fe} - i\eta)(\omega_1 - \omega_3 + \mathcal{E}_{e'e} - i\eta)|\omega_3 - \mathcal{E}_{e'g} + i\eta|^2(\omega_3 - \omega_s + i\eta)} \quad (8)$$

$$+ (\lambda_1 \Leftrightarrow \lambda_3)$$

$$R^{(5)}(\omega_s) = \sum_{\{\lambda\}} \int \frac{d\omega_1 d\omega_2 d\omega_3}{(2\pi)^3} \frac{(24i/\hbar^6)\mathcal{M}_{\lambda\lambda\lambda_1\lambda_2\lambda_3\lambda_4}^{ij;ij;ig;i'j';i'g} D_{\lambda_1\lambda_2\lambda_3\lambda_4}^{-++LRRR}(\omega_1, \omega_2, \omega_1 + \omega_2 - \omega_3, \omega_3)}{(\omega_3 - \mathcal{E}_{i'g} - i\eta)(\omega_1 + \omega_2 - \mathcal{E}_{j'g} - i\eta)|\omega_1 - \mathcal{E}_{ig} + i\eta|^2} \quad (9)$$

$$\times \frac{1}{(\omega_1 + \omega_s - \mathcal{E}_{ij} - \mathcal{E}_{ig} + i\eta)} + (\lambda_2 \Leftrightarrow \lambda_4)$$

$$R^{(6)}(\omega_s) = \sum_{\{\lambda\}} \int \frac{d\omega_1 d\omega_2 d\omega_3}{(2\pi)^3} \frac{(24i/\hbar^6)\mathcal{M}_{\lambda\lambda\lambda_1\lambda_2\lambda_3\lambda_4}^{e'g;e'g;fe;fe';eg} D_{\lambda_1\lambda_2\lambda_3\lambda_4}^{-++LRRR}(\omega_1, \omega_2, \omega_1 + \omega_2 - \omega_3, \omega_3)}{(\omega_3 - \mathcal{E}_{eg} - i\eta)(\omega_1 - \omega_3 - \mathcal{E}_{fg} - i\eta)|\omega_1 - \mathcal{E}_{e'g} - i\eta|^2(\omega_1 - \omega_s + i\eta)} \quad (10)$$

$$+ (\lambda_2 \Leftrightarrow \lambda_4)$$

where the sum over the repeated indices i, j, i', j' runs over all excited states of the molecule while sums over e, e' are restricted to the singly excited states, and $\{\lambda\}$ denotes a summation over all possible values of the polarizations for $\lambda, \lambda_i, i = 1, 2, 3, 4$. Note that $\mathcal{M}_{\lambda\lambda\lambda_1\lambda_2}^{ij;ij;ig;ig} = (\mu_{ij} \cdot \epsilon_\lambda)(\mu_{ij}^* \cdot \epsilon_\lambda)(\mu_{ig} \cdot \epsilon_{\lambda_1})(\mu_{ig}^* \cdot \epsilon_{\lambda_2})$ and $\mathcal{M}_{\lambda\lambda\lambda_1\lambda_2\lambda_3\lambda_4}^{fj;fj;fe;eg;e'g;fe'} = (\mu_{fj} \cdot \epsilon_\lambda)(\mu_{fj}^* \cdot \epsilon_\lambda)(\mu_{fe} \cdot \epsilon_{\lambda_1})(\mu_{eg}^* \cdot \epsilon_{\lambda_2})(\mu_{e'g} \cdot \epsilon_{\lambda_3})(\mu_{fe'}^* \cdot \epsilon_{\lambda_4})$, etc. The six terms in Eqs. (5) -(10) correspond to the six diagrams given in Fig. 1 in the main text.

III. NONPERTURBATIVE CALCULATION OF THE ENTANGLED-FIELD CORRELATION FUNCTIONS

Entangled ("signal-idler") photon pairs are created by the interaction of the pump field with a nonlinear PDC crystal. The entangled-field output is fully characterized by various correlations of the field operators, known as one-particle propagators that are encoded in the effective action S_{eff} of the field. The entangled-photon state is determined by the amplitude E of the pump-field and by the nonlinear (second-order $\chi^{(2)}$) response of the PDC crystal of length l along the z -axis. Extension of the crystal in the x - and y - directions is assumed to be infinite with respect to the wavelengths of the photons involved in the process. The effective action approach leads to the following effective Hamiltonian H_{eff} for the entangled-field generation.

$$H_{eff}(z) = \sum_{\alpha} \int \frac{d\omega}{2\pi} \left(\kappa_{i\alpha}(\omega) E_{i\alpha}^{\dagger}(\omega) E_{i\alpha}(\omega) + \kappa_{s\alpha}(\omega) E_{s\alpha}^{\dagger}(\omega) E_{s\alpha}(\omega) \right) + \hbar \sum_{\alpha, \beta} \int \frac{d\omega d\omega'}{(2\pi)^2} \chi^{(2)}(\omega, \omega') \mathcal{E}(\omega + \omega', z) E_{i\alpha}^{\dagger}(\omega) E_{s\beta}^{\dagger}(\omega') + h.c. \quad (11)$$

where $E_{i\alpha}^{\dagger}(\omega)$ is the creation operator in the "idler" mode with polarization ϵ_{α} , α (horizontal "H" or vertical "V"), frequency ω , $\kappa_{i\alpha}(\omega)$ is the corresponding dispersion of the mode, $\mathcal{E}(\omega, z)$ is the amplitude of the pump field at the position z along the propagation direction inside the crystal, and $\chi^{(2)}(\omega, \omega') \approx \frac{1}{2l} \sqrt{\frac{\omega_i \omega_s}{n_i n_s}} \chi_{eff}^{(2)}(\omega, \omega')$, where l is the length of the PDC crystal along the z -axis, $\omega_{i/s}(n_{i/s})$ is the central frequency (refractive index) of the idler/signal mode, and $\chi_{eff}^{(2)}$ is the second-order susceptibility of the PDC crystal. The polarization ϵ_{β} is perpendicular to ϵ_{α} , $\epsilon_{\alpha} \cdot \epsilon_{\beta} = 0$. The second term in the above Hamiltonian, therefore, generates a Bell polarization state for the signal and the idler modes.

The evolution of modes inside the crystal is determined by the Heisenberg equations,

$$\frac{\partial}{\partial z} E_{i\alpha}(\omega, z) = -\frac{i}{\hbar} \kappa_{i\alpha}(\omega) E_{i\alpha}(\omega, z) - \frac{i}{\hbar} \int \frac{d\omega'}{2\pi} \chi^{(2)}(\omega, \omega') \mathcal{E}(\omega + \omega') E_{s\beta}^{\dagger}(\omega', z) \quad (12)$$

with the initial condition $E_{i\alpha}(\omega, -l)$ defined at $z = -l$. $E_{s\alpha}$ is obtained by interchanging the indices i and s in Eq. (12).

The formal solution of Eq. (12) is

$$E_{i\alpha}(\omega, 0) = U_{ii}^{\alpha\alpha}(\omega, \omega') E_{i\alpha}(\omega', -l) + V_{is}^{\alpha\beta}(\omega, \omega') E_{s\beta}^{\dagger}(\omega', -l) \quad (13)$$

where β denotes a polarization ϵ_β perpendicular to ϵ_α . The entangled field propagators may be recast in terms of the functions $U(\omega, \omega')$ and $V(\omega, \omega')$ introduced in Eq. (13). For example, $D_{si;\alpha\alpha'}^{--LL}(\omega, \omega') \equiv \mathcal{D}_{si;\alpha\alpha'}^{--}(\omega, \omega') = \langle E_{s\alpha}(\omega) E_{i\alpha'}(\omega') \rangle$ is given by,

$$\mathcal{D}_{si;\alpha\alpha'}^{--}(\omega, \omega') = \delta_{\alpha\beta} \int \frac{d\omega_1}{2\pi} U_{ss}^{\alpha\alpha}(\omega, \omega_1, 0) V_{is}^{\alpha'\beta}(\omega', \omega_1, 0), \quad (14)$$

where $U_{ss}^{\alpha\alpha}(\omega, \omega', z)$ and $V_{is}^{\alpha\beta}(\omega, \omega', z)$ are the solutions of the coupled equations for $\tilde{U}_{ss}^{\alpha\alpha}(\omega, \omega', z) = e^{i\kappa_{s\alpha}(\omega)z} U_{ss}^{\alpha\alpha}(\omega, \omega', z)$ and $\tilde{V}_{is}^{\alpha\beta}(\omega, \omega', z) = e^{i\kappa_{i\alpha}(\omega)z} V_{is}^{\alpha\beta}(\omega, \omega', z)$,

$$\begin{aligned} \frac{\partial}{\partial z} \tilde{U}_{ss}^{\alpha\alpha}(\omega, \omega', z) &= -i \int \frac{d\omega_1}{2\pi} \chi^{(2)}(\omega, \omega_1) \mathcal{E}(\omega + \omega_1) e^{-i\Delta k_{si}^{\alpha\beta}(\omega, \omega_1)z} [\tilde{V}_{is}^{\beta\alpha}(\omega_1, \omega', z)]^* \\ \frac{\partial}{\partial z} \tilde{V}_{is}^{\alpha\beta}(\omega, \omega', z) &= -i \int \frac{d\omega_1}{2\pi} \chi^{(2)}(\omega, \omega_1) \mathcal{E}(\omega + \omega_1) e^{-i\Delta k_{is}^{\alpha\beta}(\omega, \omega_1)z} [\tilde{U}_{ss}^{\beta\alpha}(\omega_1, \omega', z)]^* \end{aligned} \quad (15)$$

with $\Delta k_{is}^{\alpha\beta}(\omega, \omega') = k_p(\omega + \omega') - \kappa_{i\alpha}(\omega) - \kappa_{s\beta}(\omega')$ and $k_p(\omega + \omega')$ being the momentum of the pump pulse at frequency $\omega + \omega'$. $\mathcal{D}_{si\alpha\alpha'}^{++}$ is obtained from (14) by replacing the field annihilation operators by the corresponding creation operators.

Note that $U^{\alpha\alpha'}$ is diagonal in the polarization indices α, α' while $V^{\alpha\beta}$ is off-diagonal. This, together with Eq. (14), implies that the propagators $\mathcal{D}_{si\alpha\alpha'}^{++}$ and $\mathcal{D}_{si\alpha\alpha'}^{--}$ are non-zero only for orthogonal polarizations ϵ_α and $\epsilon_{\alpha'}$. Similarly, $\mathcal{D}_{ss\alpha\alpha'}^{--}$ and $\mathcal{D}_{ii\alpha\alpha'}^{--}$ survive iff the α and α' polarizations are parallel. Finally, Eqs. (15) can be computed numerically for an arbitrary pump spectral envelop $\mathcal{E}(\omega)$, crystal response function $\chi^{(2)}(\omega)$, and dispersions of the pump, idler and signal modes.

Below we derive analytic expressions for a narrow pump $\mathcal{E}(\omega) = 2\pi E_p \delta(\omega_p - \omega)$ with frequency ω_p . The main simplification in this case comes from the fact that the z -dependent coefficients in the differential equation (15) drops out and the evolution inside the crystal does not require z -ordering. The ω_1 integration in Eq. (15) can be performed trivially and we finally obtain, $U_{ss}^{\alpha\alpha}(\omega, \omega', 0) = \delta(\omega - \omega') \mathcal{U}_{ss}^{\alpha\alpha}(\omega, \bar{\omega})$ and $V_{is}^{\alpha\beta}(\omega, \omega', 0) = \delta(\omega + \omega' - \omega_p) \mathcal{V}_{is}^{\alpha\beta}(\omega, \bar{\omega})$ where $\bar{\omega} = \omega_p - \omega$ and,

$$\mathcal{U}_{ss}^{\alpha\alpha}(\omega, \bar{\omega}) = e^{-i\frac{l}{2}\bar{\kappa}_{si}^{\alpha\beta}(\omega, \bar{\omega})} \left[\cosh\left(\frac{\kappa_{si}^{\alpha\beta}(\omega, \bar{\omega})l}{2}\right) + i\frac{\Delta k_{si}^{\alpha\beta}(\omega, \bar{\omega})}{\kappa_{si}^{\alpha\beta}(\omega, \bar{\omega})} \sinh\left(\frac{\kappa_{si}^{\alpha\beta}(\omega, \bar{\omega})l}{2}\right) \right] \quad (16)$$

$$\mathcal{V}_{is}^{\alpha\beta}(\omega, \bar{\omega}) = -2i\frac{E_p \chi^{(2)}(\omega, \bar{\omega})}{\kappa_{is}^{\alpha\beta}(\omega, \bar{\omega})} e^{i\frac{l}{2}\bar{\kappa}_{si}^{\beta\alpha}(\bar{\omega}, \omega)} \sinh\left(\frac{\kappa_{is}^{\alpha\beta}(\omega, \bar{\omega})l}{2}\right) \quad (17)$$

where $\bar{\kappa}_{si}^{\alpha\beta}(\omega, \omega') = k_p(\omega_p) + \kappa_{s\alpha}(\omega) - \kappa_{i\beta}(\omega')$, and

$$\kappa_{si}^{\alpha\beta}(\omega, \omega') = \sqrt{4|E_p|^2 \chi^{(2)}(\omega, \omega') \chi^{(2)}(\omega', \omega) - (\Delta k_{si}^{\alpha\beta}(\omega, \omega'))^2}.$$

$U_{ii}^{ss}(\omega, \omega', 0)$ and $V_{si}^{\alpha\beta}(\omega, \omega', 0)$ are obtained from Eqs. (16) and (17), respectively, by interchanging $i \Leftrightarrow s$.

Extension to a narrow pump pulse: The above results obtained for a CW-pump can be extended approximately for a sufficiently narrow pump pulse by using the Wigner transformation of the pulse. Assuming that the pump amplitude varies slowly enough so that the phase, which varies with frequency ω_p , is fast enough compared to the time-scale of the envelop (determined by the band-width), we extend the CW-pulse results as follows. First we re-write $U_{ss}^{\alpha\alpha}(\omega, \omega', 0) = \int dt e^{i(\omega-\omega')t} \mathcal{U}_{ss}^{\alpha\alpha}(\omega, \omega_p - \omega')$ and $V_{is}^{\alpha\beta}(\omega, \omega', 0) = \int dt e^{i(\omega+\omega'-\omega_p)t} \mathcal{V}_{is}^{\alpha\beta}(\omega, \omega_p - \omega')$. This is exact for a CW-pump for any pump amplitude, E_p . We assume that the pump amplitude E_p varies slowly enough so that E_p can be replaced by its values at different times, which makes the functions \mathcal{U} and \mathcal{V} time dependent. Thus for a narrow but finite bandwidth pump we can use,

$$U_{ss}^{\alpha\alpha}(\omega, \omega', 0) = \int dt e^{i(\omega-\omega')t} \mathcal{U}_{ss}^{\alpha\alpha}(\omega, \omega_p - \omega', t)$$

$$V_{is}^{\alpha\beta}(\omega, \omega', 0) = \int dt e^{i(\omega+\omega'-\omega_p)t} \mathcal{V}_{is}^{\alpha\beta}(\omega, \omega_p - \omega', t).$$

These equations are used to evaluate the correlation functions for a narrow pump band-widths in the main text.

A. The Two-Photon Correlation Function (TPCF) for a finite-band-width pump

The TPCF $D_{si,HV}^{--}(\omega, \omega_1)$ in Eq. 14 is evaluated numerically by solving Eqs. (15) using,

$$\Delta k_{si}^{HV}(\omega, \omega_1) = \frac{\omega - \bar{\omega}_s}{v_{1,H}} + \frac{\omega_1 - \bar{\omega}_i}{v_{2,V}} \quad (18)$$

$$\Delta k_{is}^{VH}(\omega, \omega_1) = \frac{\omega - \bar{\omega}_i}{v_{2,V}} + \frac{\omega_1 - \bar{\omega}_s}{v_{1,H}}$$

where $v_1 = v_p - v_{a,X}$, and $v_2 = v_p - v_{i,X}$ with v_p , $v_{s,X}$, and $v_{i,X}$ being group velocities of the pump, the signal, and the idler photons, respectively, with polarization ϵ_X , and $\bar{\omega}_s$ ($\bar{\omega}_i$) represents the center

frequency of the signal (idler) photon. We take $l = 20 \mu\text{m}$ crystal length, and the following spectral envelope of the pump field.

$$\mathcal{E}(\omega) = E_p e^{-(\omega_p - \omega)^2 / (2\sigma_p^2)} \quad (19)$$

where E_p , $\bar{\omega}_p$, and σ_p represent the amplitude, central frequency, and the spectral width of the field, respectively.

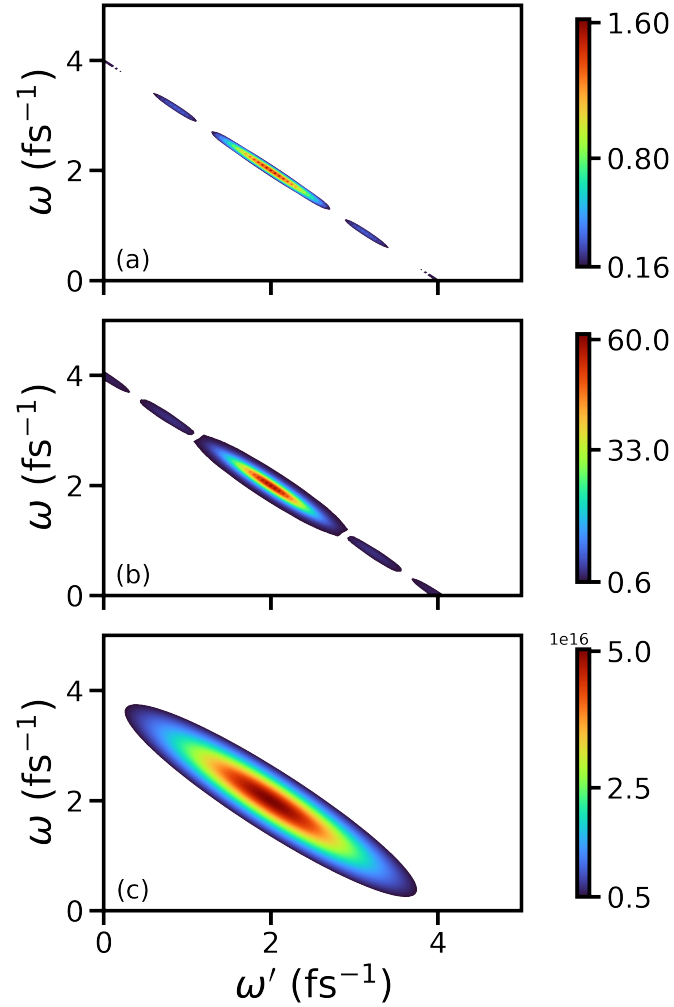


Figure 1. 2D frequency-dispersed plots for $D_{si,HV}^{--}$ (Eq. 14) with $\sigma_p = 0.1 \text{ fs}^{-1}$ and (a) $E_p = 0.01 \text{ a.u.}$, (b) $E_p = 0.1 \text{ a.u.}$, and (c) $E_p = 0.5 \text{ a.u.}$ are shown. Other system parameters: $v_{1,H} = v_{2,H} = 10 \mu\text{m} \cdot \text{fs}^{-1}$, $v_{1,V} = v_{2,V} = -10 \mu\text{m} \cdot \text{fs}^{-1}$, $\bar{\omega}_p = 10 \text{ fs}^{-1}$, and $\bar{\omega}_s = 5 \text{ fs}^{-1}$.

Figure 1 displays 2D frequency-dispersed plots for $D_{si,HV}^{--}$ for a fixed pump bandwidth of $\sigma_p=0.1\text{ fs}^{-1}$ and different pulse amplitudes (E_p). Figure 1(a) is constructed using the weakest pump with $\mathcal{E}_p=0.01$ a.u. Frequencies are clearly anti-correlated. For increased amplitude $E_p=0.1$ a.u., the signal strength increases, but the anti-correlation is still intact, as shown in Fig. 1(b). Further increase to $E_p = 1$ a.u. leads to vanishing of the features visible in the earlier two cases, as evident in Fig. 1(c). However, the frequency anti-correlation is still present in the signal. The amplitude of the correlation increases exponentially with the pump amplitude. To study the impact of the pump-

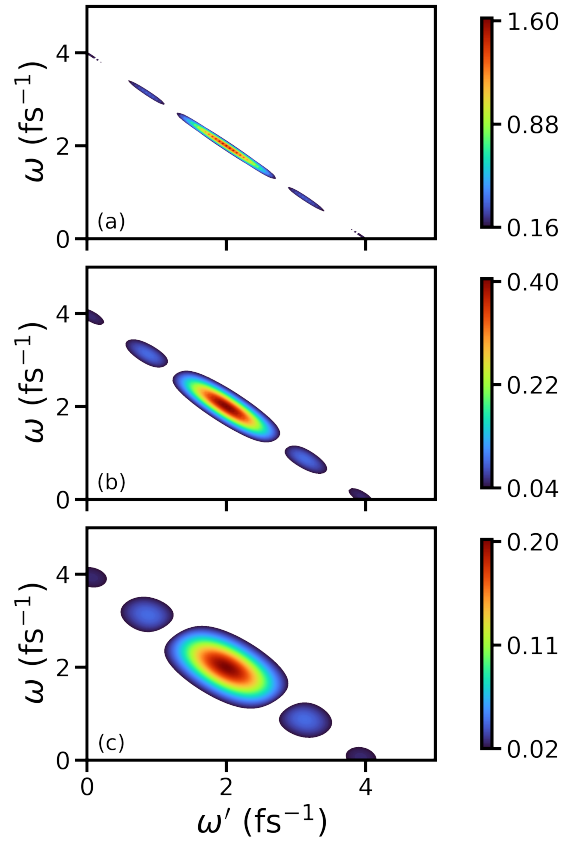


Figure 2. 2D frequency-dispersed plots for $D_{si,HV}^{--}$ (see Eq. 14) with $\mathcal{E}_p=1$ a.u., and (a) $\sigma_p=0.1\text{ fs}^{-1}$, (b) $\sigma_p=0.5\text{ fs}^{-1}$, and (c) $\sigma_p=1.0\text{ fs}^{-1}$ are shown. Other system parameters: $v_{1,H}=v_{2,H}=10\text{ }\mu\text{m}\cdot\text{fs}^{-1}$, $v_{1,V}=v_{2,V}=-10\text{ }\mu\text{m}\cdot\text{fs}^{-1}$, $\bar{\omega}_p=10\text{ fs}^{-1}$, and $\bar{\omega}_s=5\text{ fs}^{-1}$.

width on the frequency anti-correlation, we present in Fig. 2 frequency dispersed plots of $D_{si,HV}^{--}$ for

a fixed pump amplitude but different band-widths. For a narrowband pump with $\sigma_p=0.1 \text{ fs}^{-1}$, the frequency anti-correlation is still present, although limited to the central blob, as shown in Fig. 2(a). However, for a larger pulse width with $\sigma_p=1 \text{ fs}^{-1}$, the signal spreads into the entire frequency range with weak features of anti-correlation, as shown in Fig. 2(b). For a broadband pulse with $\sigma_p=1 \text{ fs}^{-1}$, the frequency entanglement vanishes and the signal covers the entire frequency range with no signs of anti-correlation, as evident in Fig. 2(c). In addition, as can be seen by comparing the three panels in Fig. 2, the intensities increase significantly with the pulse width.

B. $g^{(2)}(\tau)$ with zero bandwidth pump pulse

For a zero-band-width pump, Eqs. (16) and (17) can be solved for the dynamical Eq. (15). $D_{si\alpha\alpha'}^{--}(\omega, \omega')$ in Eq. (14) may be then expressed as (we remove polarization indices assuming that the "idler" and "signal" modes have fixed orthogonal polarizations),

$$D_{si}^{--}(\omega, \omega') = -\frac{2i}{h}\delta(\omega + \omega' - \omega_p)\frac{\chi^{(2)}E_p}{\kappa_{is}(\omega\bar{\omega})}e^{-i\frac{l}{2}(\bar{\kappa}_{si}(\omega, \bar{\omega}) - \bar{\kappa}_{si}(\bar{\omega}, \omega))}\sinh\left(\frac{l}{2}\kappa_{is}(\bar{\omega}, \omega)\right) \\ \times \left(\cosh\left(\frac{l}{2}\kappa_{si}(\omega, \bar{\omega})\right) + i\frac{\Delta k_{si}(\omega, \bar{\omega})}{\kappa_{si}(\omega, \bar{\omega})}\sinh\left(\frac{l}{2}\kappa_{si}(\omega, \bar{\omega})\right)\right) \quad (20)$$

where $\bar{\omega} = \omega_p - \omega$ and the phase miss-match $\Delta k_{si}(\omega, \bar{\omega})$ is approximated using Taylor expansion $\kappa_{s\alpha}(\omega) \sim \kappa_{s\alpha}(\omega_s) + (\omega - \omega_s)T_{s\alpha}/l$ and $\kappa_{i\alpha}(\omega') \sim \kappa_{i\alpha}(\omega_i) + (\omega - \omega_i)T_{i\alpha}/l$ around the central frequencies ω_i and ω_s of the "idler" and "signal" photons, respectively, to obtain, $\Delta k_{si}(\omega, \bar{\omega}) \approx -\frac{\Delta T}{l}(\omega - \omega_s)$ and $\Delta k_{is}(\omega, \bar{\omega}) \approx \frac{\Delta T}{l}(\omega - \omega_i)$ with $\Delta T = T_s - T_i$ being the entanglement time. Similarly, for the intra-mode correlations, we get

$$D_{ii}^{+-}(\omega, \omega') = 4\delta(\omega - \omega')\left|\frac{E_p\chi^{(2)}}{\kappa_{si}(\omega, \bar{\omega})}\sinh\left(\frac{\kappa_{si}(\omega, \bar{\omega})}{2}l\right)\right|^2. \quad (21)$$

Note that for the narrow band-width pump, all intra-mode (inter-mode) propagators are diagonal (anti-diagonal) in the frequency space. This allows us to simplify the expression for $g^{(2)}(\tau)$ using Eq.

(6) in the main text.

$$\begin{aligned}
g^{(2)}(\tau) &= 1 + \frac{1}{S(\tau)} \int \frac{d\omega d\omega'}{(2\pi)^2} \sum_{qq'=i,s} D_{qq}^{+-}(\omega, \omega) D_{q'q'}^{+-}(\omega', \omega') e^{-i(\omega-\omega')\tau} \\
&+ \sum_{q \neq q'} \sum_{q_1 \neq q'_1} \frac{1}{S(\tau)} \int \frac{d\omega d\omega'}{(2\pi)^2} D_{qq'}^{++}(\omega, \omega) D_{q_1 q'_1}^{--}(\omega', \omega') e^{i(\omega_p - \omega - \omega')\tau}. \tag{22}
\end{aligned}$$

For simplicity, we assume a degenerate PDC process $\omega_i = \omega_s$. In this case, $g^{(2)}(\tau)$ simplifies to,

$$\begin{aligned}
g^{(2)}(\tau) &= 1 + \frac{1}{S(\tau)} \left(\frac{8(\chi E_p l)^2}{\Delta T} \right)^2 \left| \int \frac{d\omega}{2\pi} \frac{\sinh^2(\frac{1}{2}\sqrt{(2\chi E_p l)^2 - \omega^2})}{(2\chi E_p l)^2 - \omega^2} e^{i\omega \frac{\tau}{\Delta T}} \right|^2 \\
&+ \frac{1}{S(\tau)} \left(\frac{2\chi E_p l}{\Delta T} \right)^2 \left| \int \frac{d\omega}{2\pi} \frac{\sinh(\sqrt{(2\chi E_p l)^2 - \omega^2})}{\sqrt{(2\chi E_p l)^2 - \omega^2}} e^{i\omega \frac{\tau}{\Delta T}} \right|^2 \\
&\approx 1 + \frac{1}{\pi S(\tau)} \left(\frac{(\sinh(\chi E_p l))^2}{\alpha_1 \Delta T} \right)^2 e^{-\frac{1}{2} \left(\frac{\tau}{\alpha_1 \Delta T} \right)^2} + \frac{1}{2\pi S(\tau)} \left(\frac{\sinh(2\chi E_p l)}{\alpha_2 \Delta T} \right)^2 e^{-\frac{(\tau+\tau_0)^2 + (\tau-\tau_0)^2}{(\alpha_2 \Delta T)^2}} \tag{23}
\end{aligned}$$

where in the second line we have used the approximation of steepest descent method to evaluate the integral, $\alpha_n = \sqrt{n\chi E_p l \coth(n\chi E_p l) - 1}/(2\chi E_p l)$, $n = 1, 2$, and $\tau_0 = T_i + T_s$. The normalization $S(\tau) = \mathcal{S}^2$ is independent of delay with $\mathcal{S} = 2 \int \frac{d\omega}{2\pi} |V_{si}(\omega, \omega)|^2$, which gives, $\mathcal{S} = \frac{(\sinh(\chi E_p l))^2}{\sqrt{\pi} \alpha_1 |\Delta T|}$. Substituting this in the above equation for $g^{(2)}(\tau)$, we get

$$g^{(2)}(\tau) = 1 + e^{-\frac{1}{2} \left(\frac{\tau}{\alpha_1 \Delta T} \right)^2} + 2 \left(\frac{\alpha_1 \coth(\chi E_p l)}{\alpha_2} \right)^2 e^{-\frac{(\tau+\tau_0)^2 + (\tau-\tau_0)^2}{(\alpha_2 \Delta T)^2}}. \tag{24}$$

The intra-mode contribution decays to unity while the inter-mode contribution decays to zero at large τ . For $\tau = 0$, the intra-mode part is independent on the pump intensity and is equal to 2, while the inter-mode contribution decays rapidly with increasing pump intensity for small values of pump intensities, $E_p < 1/(\chi l)$, and saturates to unity for large pump intensities.